AGU PUBLICATIONS

JGR

Journal of Geophysical Research: Oceans

RESEARCH ARTICLE

10.1002/2013JC009050

Key Points:
- Chlorophyll response to El Nino using a coupled model
- Different spatial-temporal response of chlorophyll for two types of El Nino
- Identification of physical factors for chlorophyll concentration

Correspondence to:
S.-W. Yeh,
swyeh@hanyang.ac.kr

Citation:
Lee, K.-W., S.-W. Yeh, J.-S. Kug, and J.-Y. Park (2014), Ocean chlorophyll response to two types of El Niño events in an ocean-biogeochemical coupled model, *J. Geophys. Res. Oceans*, *119*, 933–952, doi:10.1002/2013JC009050.

Received 26 APR 2013
Accepted 13 JAN 2014
Accepted article online 16 JAN 2014
Published online 12 FEB 2014

Ocean chlorophyll response to two types of El Niño events in an ocean-biogeochemical coupled model

Kie-Woung Lee[1], Sang-Wook Yeh[1], Jong-Seong Kug[2], and Jong-Yeon Park[3]

[1]Department of Marine Sciences and Convergent Technology, Hanyang University, Ansan, South Korea, [2]School of Environmental Science and Engineering, Pohang University of Science and Technology, [3]Max Planck Institute for Meteorology, Hamburg, Germany

Abstract Based on a long-term simulation of an ocean-biogeochemical coupled model, we investigate the biogeochemical response to the two types of El Niño events, a Cold Tongue (CT)-El Niño and a Warm Pool (WP)-El Niño, in which a local maximum of anomalous sea surface temperature (SST) is located in the eastern and central tropical Pacific. Our model is able to reasonably simulate the characteristics of the biological variables in a way comparable to the observations. During the developing period, anomalous low chlorophyll appears in the eastern Pacific, while it appears in the central Pacific in the WP-El Niño. The difference in the spatial-temporal response of chlorophyll for the two types of El Niño events is mainly due to the eastward zonal advection of upper ocean currents, which plays a role in bringing nutrient-poor water from the western Pacific. During the decaying period of the WP-El Niño, anomalous high chlorophyll appears concurrently with anomalous low SST in the eastern Pacific. Conversely, anomalous high chlorophyll appears in the central Pacific prior to the decaying period of the CT-El Niño. In particular, the anomalous low sea level from the northwestern Pacific shifts to the southern equatorial region during the decaying period of the CT-El Niño. This drives anticyclonic boundary currents which enhance the Equatorial Undercurrent, playing a role in the supply of nutrients to the central equatorial Pacific, resulting in an increase in chlorophyll concentration in the same region.

1. Introduction

Phytoplankton are one of the primary producers in the ecosystem via carbon fixation, producing nearly half of the world's oxygen through photosynthesis. They assist in recycling elements such as carbon, phosphorus, and nitrogen, which are required by other organisms [*Field et al*., 1998; *Behrenfeld et al*., 2001]. Typically, chlorophyll is used to measure the concentration of biomass, such as phytoplankton and algae. Furthermore, chlorophyll affects the absorption of shortwave radiation and, thus, the vertical distribution of ocean temperature in the upper ocean [*Lewis et al*., 1983, 1990; *Siegel et al*., 1995], which is able to modify air-sea interaction processes. Therefore, an understanding of how the variability of chlorophyll is associated with the changes in the physical properties of the upper ocean sheds light on many topics.

The concentration of chlorophyll is determined by the light, temperature, and nutrients available [*Tilman et al*., 1982; *Cullen*, 1991]. The Equatorial Pacific region is characterized by richer light and temperature, but less of the nutrients that are needed for the growth of phytoplankton. In more detail, the nutrient requirements within the equatorial Pacific differ considerably (e.g., iron limited, nitrate replete in eastern Pacific versus iron replete, nitrate limited in western Pacific) [*Landry et al*., 1997; *Radenac et al*., 2001]. Thus, the supply of nutrients including iron and nitrate is important for the increase of chlorophyll in the equatorial Pacific.

Previous studies have shown that the variability of chlorophyll is associated with climate variability on intraseasonal-to-decadal time scales, such as: the Madden Julian Oscillation, tropical cyclone activity, El Niño-Southern Oscillation (ENSO), and Pacific Decadal Oscillation (PDO) [*Mantua et al*., 1997; *Chavez et al*., 1999, 2003; *Turk et al*., 2001; *Yoder and Kennelly*, 2003; *Dandonneau et al*., 2004; *Yeh et al*., 2011; *Jin et al*., 2013]. Furthermore, numerous studies have shown that the concentration of chlorophyll decreases in the eastern and central Pacific during El Niño events (and increases during La Niña events) [*Ryan et al*., 2006; *Turk et al*., 2011; *Radenac et al*., 2012]. This is because the change in nutrient supply, which is a key factor in controlling the amount of chlorophyll, is largely associated with the changes in thermocline depth,

nutricline, and the upward vertical nutrient flux in the eastern equatorial Pacific during ENSO events. Moreover, the zonal advection of nutrient-poor/warm pool and nutrient-rich/cold tongue regions is also important in controlling chlorophyll variability during ENSO events [*Blanchot et al*., 1992; *Chavez et al*., 1991, 1999; *Radenac et al*., 2005; *Ryan et al*., 2006]. Thus, ENSO plays a key role in influencing the variability of chlorophyll in the tropical Pacific ecosystem.

Recently, many studies have suggested that there exist two types of El Niños. A new type of El Niño (referred to as a Central Pacific El Niño, Dateline El Niño, El Niño Modoki, or Warm pool El Niño) differs from the conventional El Niño (referred to as an Eastern Pacific El Niño, Cold tongue El Niño, or Canonical El Niño) in terms of spatial pattern and evolution of SST [*Trenberth and Stepaniak*, 2001; *Ashok et al*., 2007; *Kao and Yu*, 2009; *Kug et al*., 2009]. Hereafter, we refer to the new type of El Niño as a Warm pool El Niño (WP-El Niño) and the conventional El Niño as a Cold tongue El Niño (CT-El Niño) following *Kug et al*. [2009]. Positive SST anomalies have occurred both in the eastern and central Pacific during CT-El Niños; however, they have been confined to the central Pacific during WP-El Niños. In addition to the SST anomalies, the spatial and temporal patterns of the other dynamic fields are distinctly different between the two types of El Niño, according to previous studies [*Kao and Yu*, 2009; *Kug et al*., 2009, 2010]. Therefore, such changes in El Niño patterns may lead to changes in biological responses in the tropical Pacific basin.

Since the 1990s, WP-El Niños have occurred more frequently and intensively [*Lee and McPhaden*, 2010] and may continue to occur more frequently under global warming [*Yeh et al*., 2009; *Yu et al*., 2012]. There have been several recent studies which examine the response of tropical ecosystems to WP-El Niños [*Turk et al*., 2011; *Radenac et al*., 2012; *Gierach et al*., 2012]. The results of these studies showed that negative chlorophyll anomalies exist in the central Pacific only during WP-El Niños. The difference in the spatial pattern of the chlorophyll anomalies for the two types of El Niños is, arguably, dependent on the strength and extent of westerly wind anomalies associated with the amplitude of the El Niños [*Turk et al*., 2011; *Gierach et al*., 2012] and their impact on horizontal and vertical processes. Horizontal advection is a primary contributor to the differences in the chlorophyll concentrations of the two types of El Niño events in the central equatorial Pacific, whereas vertical advection and mixing is a dominant process in the eastern equatorial Pacific [*Gierach et al*., 2012]. In detail, westward surface currents in the central Pacific limit the expansion of anomalous chlorophyll core during WP-El Niño events and negative chlorophyll anomalies that extend eastward, which is mainly due to reduced upward iron fluxes linked to the deepening of the Equatorial Undercurrent [*Radenac et al*., 2012].

In spite of these studies, it is still important to investigate the biological response in the equatorial Pacific Ocean in terms of the detail of relevant physical processes. This is because most previous studies have relied predominantly on satellite observation data only useful since 1997. Therefore, only two cases for CT-El Niño events (1997–1998, 2006–2007) and three cases for WP-El Niño (2002–2003, 2004–2005, and 2009–2010) events have been observed since 1997. The time period analyzed is limited in these studies due to the length of the continuous ocean color record (i.e., 1997 to present). Therefore, it is very useful to examine details of physical processes on the chlorophyll response to two types of El Niño using a long-term simulation in a coupled model. The purpose of this study is to examine the mechanisms of the nutrients supply process associated with the amount of chlorophyll during the developing or decaying period in the two types of El Niño based on a long-term ocean-biogeochemical coupled model simulation using Geophysical Fluid Dynamics Laboratory Modular Ocean Model Version4 (GFDL MOM4p1).

A detailed explanation of the model used is provided in section 2. We discuss the chlorophyll responses to the two types of El Niño events and the physical process in section 3. A summary is given in section 4.

2. Model and Data

We analyze a biogeochemical and ocean ecosystem model, developed at GFDL, with the MOM4 [*Griffies et al*., 2009; *Gnanadesikan et al*., 2006]. The ocean model has 50 vertical *z* coordinates and a spatial resolution of nominally 1° globally, with a higher 1/3° resolution near the equator. The vertical resolution is nonuniform. The resolution is uniform with a grid spacing of 10 m in the upper level from the depth of 5–235 m, whereas the grid interval linearly increases from the depth of 366 m to the bottom. The mixed layer depth (MLD) in the model is defined as the depth where the buoyancy difference from the surface is 0.0003

ms^{-2}. In our model experiments, the optical routine used for estimating shortwave penetration, representing the impact of chlorophyll on the optical properties of ocean water, is the Manizza optics scheme [*Manizza et al*., 2005]. Thickness and density weighted tendency of temperature associated with penetrative shortwave heating is computed from either implemented chlorophyll data or a biogeochemical model. In this scheme, the shortwave radiation is computed at every vertical level of the model as a function of the chlorophyll concentration and the irradiance at the vertical level just above. Thus, this scheme considers the self-shading effect caused by the presence of phytoplankton in the water column.

The biogeochemical model for the simulation of chlorophyll concentration is the Tracers of Phytoplankton with Allometric Zooplankton (TOPAZ) model [*Geider et al*., 1996; *Dunne*, 1999; *Dunne et al*., 2005]. The TOPAZ model was designed to represent the phytoplankton functional groups of (1) a small (picoplankton/nanoplankton) group caught in a tight microbial loop loosely characterized as cyanobacteria and (2) a large (nanoplankton and microplankton) group of phytoplankton capable of being decoupled from grazing and to create sinking material. The latter are facultatively (3) diatoms. This serves as an alternative to explicitly represent diatoms as the only exportable form of primary production after *Dunne et al*. [2000]. This model is coupled with the ocean model (MOM4p1) and it considers 25 tracers, including three phytoplankton groups, two forms of dissolved organic matter, heterotrophic biomass, and dissolved inorganic species. The phytoplankton functional groups undergo colimitation by light, nitrogen, phosphorus, and iron with flexible physiology, but each phytoplankton group has its own parameter set for determining growth rates and its own nutrient stoichiometry. The growth rates for phytoplankton are modeled as a function of variable chlorophyll to carbon ratios. A key feature of the model is the parameterization of phytoplankton loss through the size-based relationship. The TOPAZ model has been tested against global nutrient and satellite observations in the GFDL global ocean model, and has shown a good performance in simulating observational biogeochemical properties [*Henson et al*., 2009; *Gnanadesikan et al*., 2011].

The TOPAZ divides the phytoplankton community into a small number of functional groups that react differently to light and nutrient limitations. The growth rate (μ) of a given group of phytoplankton is:

$$\mu = \frac{P^{C}_{max}}{1+\zeta} e^{kT} \min\left(\mathrm{Lim}_{N}, \mathrm{Lim}_{P}, \mathrm{Lim}_{Fe}\right) \times \mathrm{Lim}_{Irr}$$

where P^{C}_{max} is the maximum carbon assimilation rate (s^{-1}), ζ is the cost of biosynthesis (set to 0.1), k is the eppley temperature coefficient (0.063 K^{-1}), T is the temperature (K), and $\mathrm{Lim}_{(N,P,Fe,Irr)}$ refer to the limitation terms for nitrogen, phosphorus, iron, and light, respectively. Phytoplankton is then influenced by temperature, whatever nutrient is most limiting, and by light. The physiological limitations of each term are described in detail in *Dunne et al*. [2010].

In our present study, the GFDL MOM4 with TOPAZ is forced by the historical wind, derived from the National Centers for Environmental Prediction-National Center for Atmospheric Research (NCEP-NCAR) reanalysis 1 [*Kalnay et al*., 1996], for the period of 1951–2010. We limited the period analyzed to 1971–2010, because of the spin-up time before 1970. We used climatological boundary conditions, including: shortwave radiation, longwave radiation, near-surface specific humidity, and air temperature. These climatological boundary conditions are obtained from the Common Ocean-ice Reference Experiment (CORE) forcing data set [*Large and Yeager*, 2004]. Runoff is given by a climatological annual value, and wet and dry dust deposition fluxes are prescribed by the monthly climatology from *Ginoux et al*. [2001]. Recent studies used the TOPAZ model to examine the marine biological feedback in both the tropics and the global ocean [*Gnanadesikan et al*., 2011; *Park and Kug*, 2013; J.-Y. Park et al., A modeling study on bio-physical processes associated with ENSO, submitted to *Progress in Oceanography*, 2014].

The observed chlorophyll concentrations are derived from measurements taken using the Sea-viewing Wide Field-of-view Sensor (SeaWiFS; 1997–2002) and the Moderate Resolution Imaging Spectroradiometer (MODIS; 2003–2010) aboard the Aqua satellite. We used 9 km resolution monthly composites, *provided* by the NASA Goddard Space Flight Center (GSFC) and Distributed Active Archive Center (DAAC) [*Campbell et al*., 1995; *McClain et al*., 2004]. The SST data used in this study is NOAA Extended Reconstructed SST (ERSST) V3b [*Smith et al*., 2008]. The ERSST is on a $2^{\circ} \times 2^{\circ}$ (latitude $\times$ longitude) grid and covers 40 years, from 1971 to 2010. We interpolated the observation data onto a $1^{\circ} \times 1^{\circ}$ grid using a bilinear interpolation method.

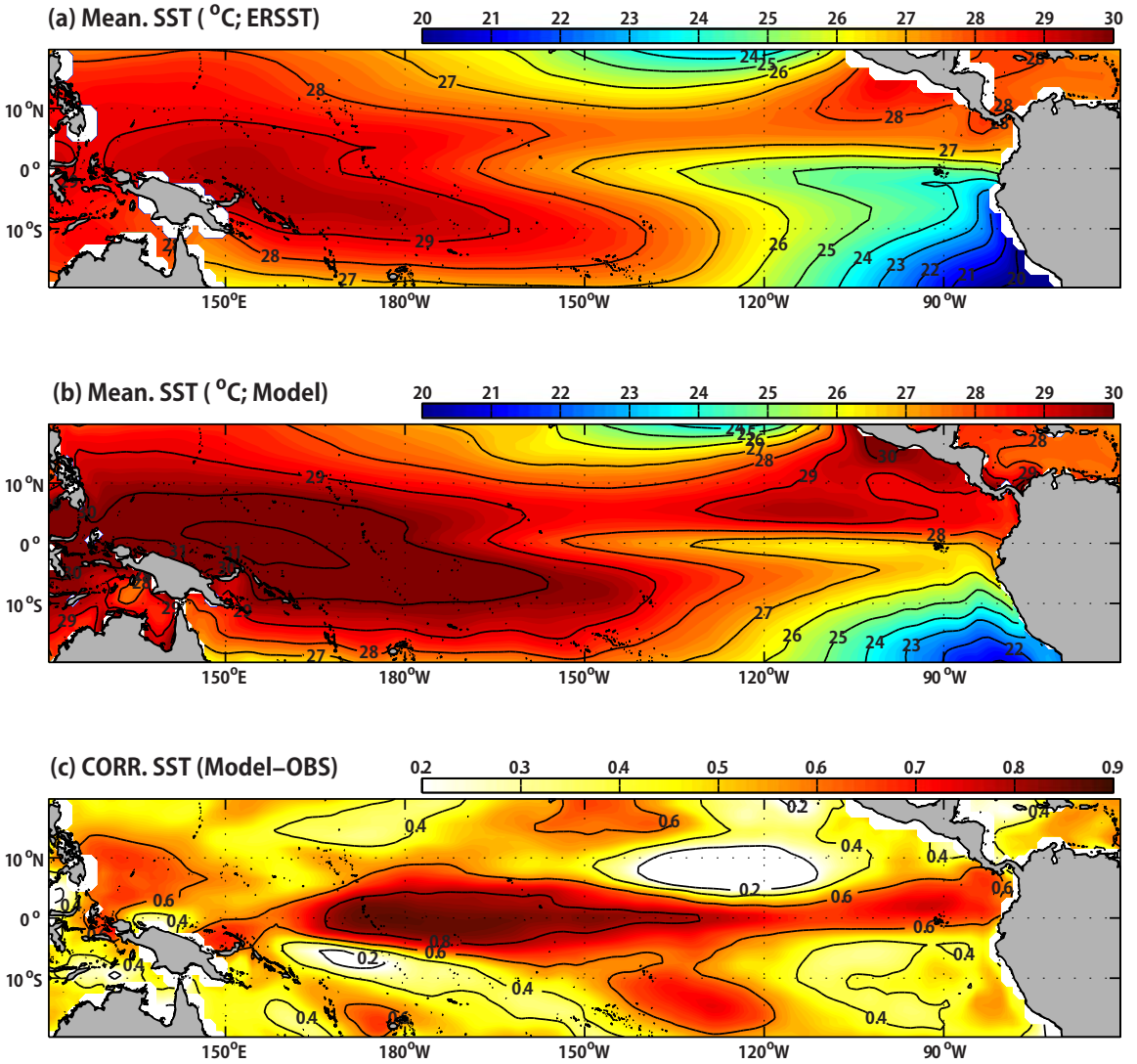

Figure 1. Model performance. The mean of SST for ERSST (a) V3b and (b) model during 1971–2010. (c) SST anomaly correlation map between model and ERSST V3b.

3. Results

3.1. Model Validation

Prior to examining the chlorophyll responses to the two types of El Niño events, we compare the model performance with the observations in terms of oceanic mean states and their interannual variability. Figures 1a and 1b show the observed SST climatology and the model simulation during 1971–2010, respectively. The simulated mean SST shows a spatial pattern that is similar to what is observed. However, the model tends to simulate the SST approximately 2°C warmer than what is observed, possibly due to a simple heat flux parameterization. Conversely, the model is able to reasonably capture the interannual variability of the SST. Figure 1c provides the temporal correlation coefficients between the observed and model monthly SST anomalies for the years 1971–2010. The correlation coefficients are higher than 0.6 in most regions in the tropical Pacific. Specifically, the correlation coefficients in the Niño3 region (5°N–5°S, 90°W–150°W), Niño3.4 region (5°N–5°S, 120°W–170°W), and Niño4 region (5°N–5°S, 150°W–160°E) are 0.8, 0.87, and 0.91, respectively, which are statistically significant at 95% confidence level using the *t* test [*Livezey and Chen*, 1983]. These results indicate that the ocean model, forced by a historical wind stress forcing, is able to reasonably simulate the SST variability on an interannual time scale.

Furthermore, we compare the SST patterns along with surface wind for both types of El Niño events during the boreal winter (December-January-February, DJF) between the model simulation and the observations

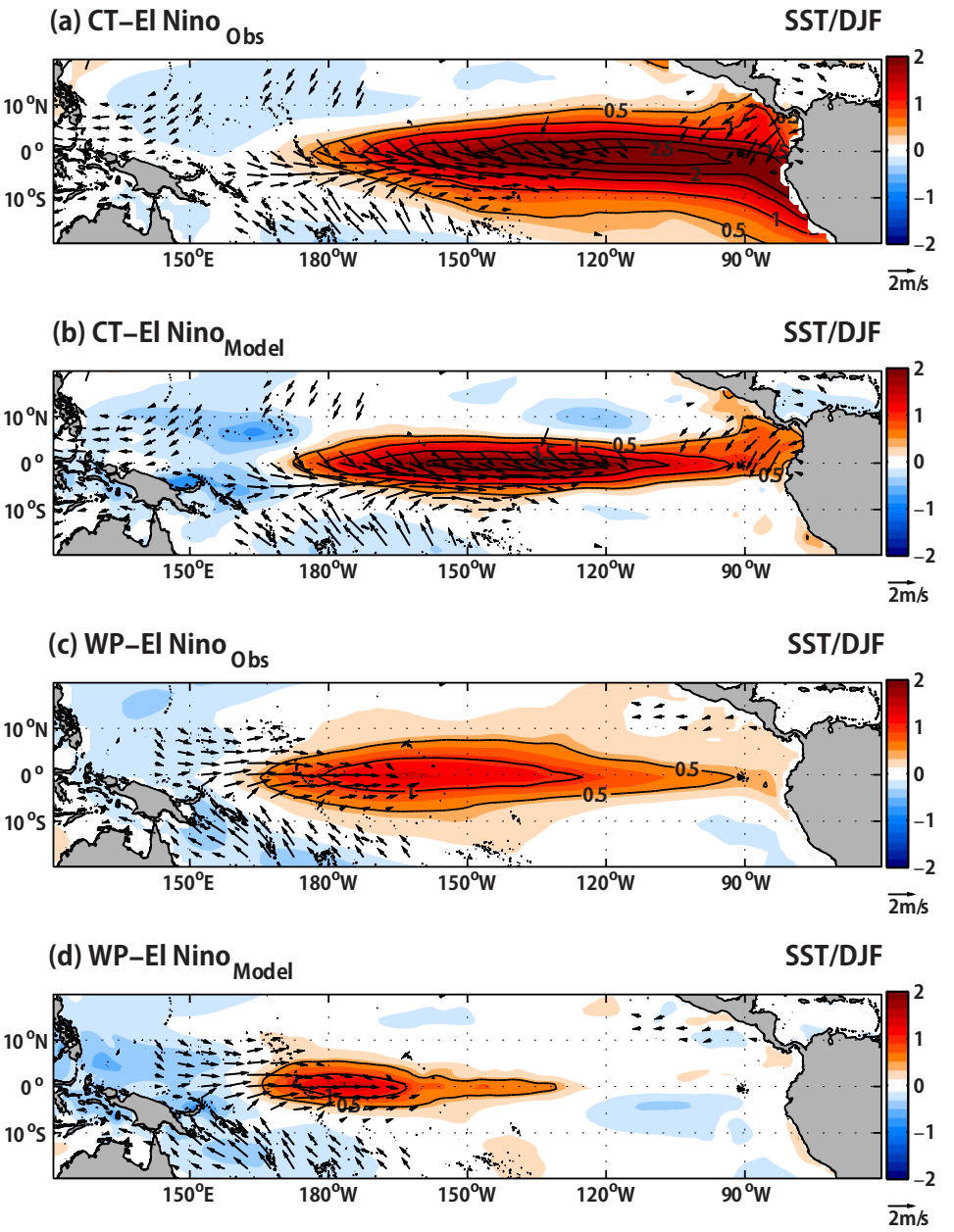

Figure 2. SST anomaly composite (°C) during winter season (DJF; 1971–2010) of El Niño events; (a) CT-El Niño for ERSST, (b) CT-El Niño for model, (c) WP-El Niño for ERSST, and (d) WP-El Niño for model. Contour interval is 0.5°C. Dotted areas denote 95% confidence regions. Scale vector indicates 2 m/s. Only surface winds with velocity >0.5 m/s are shown.

(Figure 2). We adopt the definitions of the CT-El Niño and WP-El Niño from *Kug et al*. [2009]. To classify the two types of El Niño, the years when either Niño3 SST or Niño4 SST from September to the following February is greater than its corresponding standard deviation are selected. Among those years, the CT-El Niño is defined when Niño3 SST is greater than the Niño4 SST and the WP-El Niño is defined when the Niño4 SST is greater than the Niño3 SST. The years with occurrences of the two types of El Niño events, as seen in observations and simulated by our model, are depicted in Table 1.

During a CT-El Niño, a center of maximum positive anomalies is observed east of 180° along with strong westerlies from the western and central tropical Pacific (Figure 2a); however, it is located in the central tropical Pacific during the observed WP-El Niño with westerlies confined in the western tropical Pacific (Figure 2c). Compared to the observed features, the model has similar patterns and magnitudes of SST anomalies. Note that the model is forced by the historical wind; therefore, the spatial structures of surface wind

Table 1. Classification of El Niño Events Into WP-El Niño (WP) or CT-El Niño (CT) From 1971 to 2010[a]

Year	1972–1973	1976–1977	1977–1978	1982–1983	1990–1991	1994–1995	1997–1998	2002–2003	2004–2005	2006–2007	2009–2010
Classification	CT	CT	WP	CT	WP	WP	CT	WP	WP	CT	WP

[a]SONDJF SST composites; CT: Ni∼no-3>1 standard deviation and standardized Ni∼no-3>standardized Ni∼no-4; WP: Ni∼no-4>1 standard deviation and standardize Ni∼no-4>standardized Ni∼no-3.

forcings are identical with the observations. However, the model tends to simulate the center of maximum positive anomalies westward for both types of El Niño events (Figures 3b and 3d). That is, the center of the maximum SST is shifted to the west approximately 20°–30°. In addition, it appears that the meridional scale of SST is narrower in the model simulation than in the observations. It is well known that most current climate models have a systematic problem that the center of the maximum SST is shifted to the west, which is mainly associated with the equatorial SST bias [*AchutaRao and Sperber*, 2002; *Hannachi et al*., 2003; *Wittenberg et al*., 2006; *Kug et al*., 2010]. Despite these differences, the model tends to simulate the features distinguishing the two types of El Niño events. In particular, it is evident that the center of the maximum anomalous SST of the WP-El Niño shifted westward approximately 30° compared to that of the CT-El Niño.

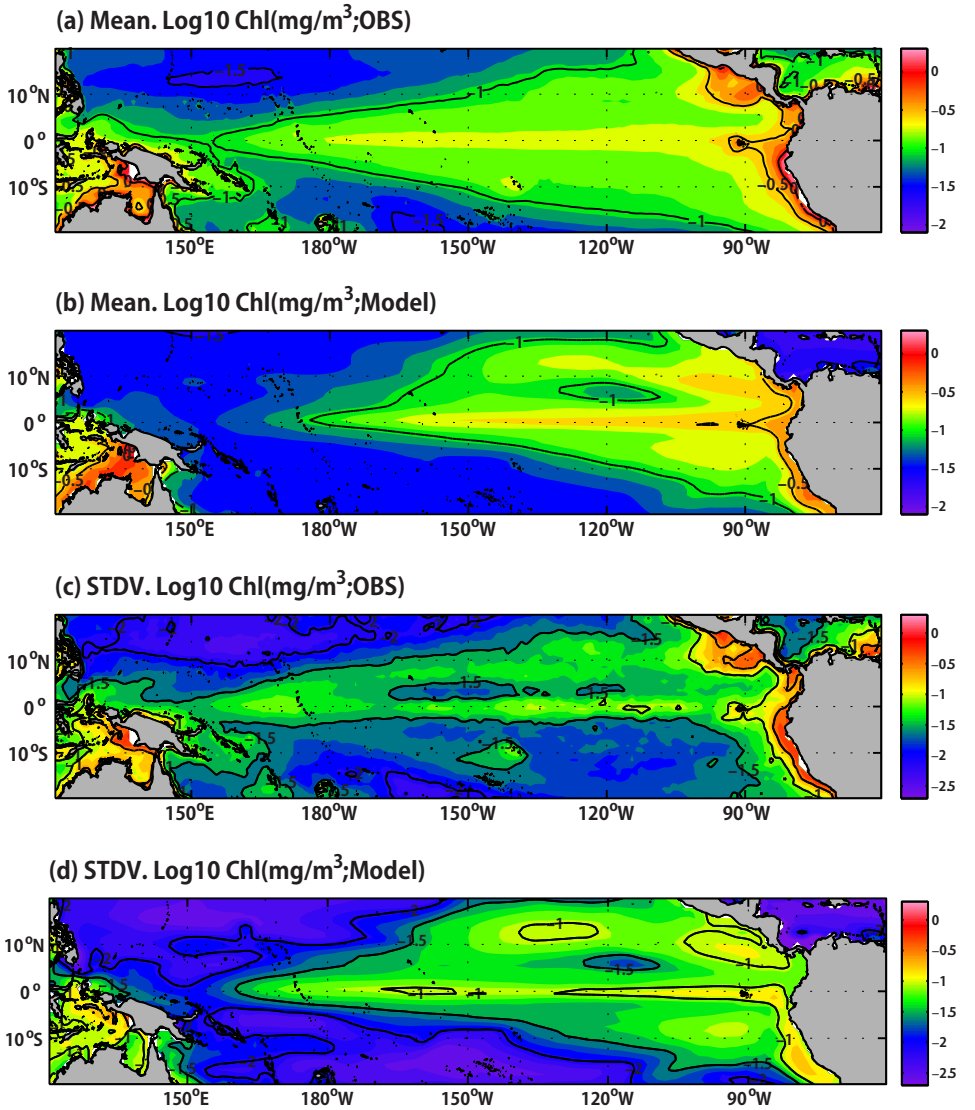

Figure 3. (a) The mean concentration of chlorophyll for observation for the period of 1997–2010. (b) Same as in Figure 3a except the model. (cand d The standard deviation of chlorophyll for observation (1997–2010) and model (1971–2010). Note that mean and standard deviation of chlorophyll was expressed as a log10 scale.

We also examine the model performance in simulating the biological variables. Figure 3 shows the long-term mean chlorophyll concentration observed from 1997 to 2010 compared to the model simulation for the years 1971–2010. Note that the chlorophyll concentration is obtained from the surface in the model, which is comparable to the observations. The correlation coefficients in chlorophyll concentration averaged in the Niño3 region and Niño4 region are 0.44 and 0.70, respectively, for the period of 1997–2010, which are statistically significant at 95% confidence level. The chlorophyll concentration is high in the eastern Pacific and low in the western Pacific in both the observation (Figure 3a) and the model (Figure 3b) [*Radenac et al*. 2013]. In particular, a higher concentration is located in the equatorial eastern coastal regions. This is predominantly because of the coastal upwelling, which shifts cool and nutrient-rich waters toward the upper ocean. The simulated mean chlorophyll concentration is lower than the observed concentration in the eastern coastal region. The mean concentration and interannual variability show higher values near islands (e.g., Marquesas Island and Kiribati Island) in the observation (Figures 3a and 3c). The shallow topography close to islands enhances the vertical mixing locally and breaks down the pycnocline (nutricline). Furthermore, eddies on the downstream side of the island that form in both the tidal and steady currents, the so-called Island mass effect [*Doty and Oguri*, 1956; *Martinez and Maamaatuaiahutapu*, 2004], is not represented well in the model (Figures 3b and 3d). In addition, the phytoplankton groups defined with TOPAZ may have some contribution to the disagreement with satellite observations. Nevertheless, the model tends to simulate the distribution of the chlorophyll concentration fairly accurately and its interannual variability, compared to the observations, shows that the model simulation can be used to examine the biological response to two types of El Niño events.

Figure 4 displays the composite chlorophyll concentration along with the surface winds for both types of El Niño events during the boreal winter (Figures 4a–4d). The chlorophyll anomalies seem to have two distinct cores (<-0.05 mg/m^3) in the CT-El Niño, seen in both the observation (Figure 4a) and the model (Figure 4b). One appears between the 180°W and 110°W in the central equatorial Pacific, and the other is east of 100°W, in the eastern equatorial Pacific. The reasons why the negative anomalies of chlorophyll concentration are dominant in the central and eastern equatorial Pacific during the CT-El Niño have been previously discussed [*Chavez et al*., 1998; *Radenac et al*., 2001]. In short, a weakening of the trade winds and the consequent thermocline deepening leads to a reduction in the amounts of nutrients in the eastern equatorial Pacific. In addition, a relatively low concentration of nutrient and chlorophyll water in the western equatorial Pacific is advected to the central equatorial Pacific due to an anomalous eastward current, which is responsible for the reduction in the chlorophyll concentration. It is evident that there exist strong westerlies in the western and central equatorial Pacific, which play a role to the advection of low concentration of nutrient and chlorophyll water from the western equatorial Pacific. Conversely, the chlorophyll anomalies associated with the WP-El Niño exhibit one core (<-0.05 mg/m^3) near the date line in both the observation (Figure 4c) and the model (Figure 4d), indicating that an eastward zonal advection of less concentration of nutrient water due to the westerlies in the western equatorial Pacific plays a role in reducing the concentration of chlorophyll during WP-El Niño events. In contrast, there is little signal of anomalous low chlorophyll in the eastern equatorial Pacific, which is quite different from the CT-El Niño. These results are similar with previous studies based on observations [*Turk et al*., 2011; *Radenac et al*., 2012; *Gierach et al*., 2012]. The details of these processes will be discussed in the next subsection.

3.2. Physical Processes

3.2.1. Seasonal Evolution

In order to examine the mechanisms behind chlorophyll concentration in response to the two types of El Niño events, we first show the evolution of the surface zonal current anomalies associated with the two types of El Niño events (Figures 5a and 5b). One may argue that the Hovmuller plots are likely biased by the strongest El Niño event such as 1997/1998 and may not be representative of all events; however, there is little difference of those Hovmuller plots with and without 1997/1998 in the present study (not shown).

In the CT-El Niño (Figure 5a), anomalous eastward currents exist in the whole equatorial Pacific basin and their maximums appear during the developing period (i.e., September(0)-October(0)-November(0), SON(0)). Subsequently, the eastward zonal current diminishes abruptly around December(0) and its direction changes westward during the peak period of the CT-El Niño. In contrast, the eastward zonal currents associated with the WP-El Niño (Figure 5b), which are confined to the western and central equatorial Pacific, are the strongest during its peak period (i.e., December(0)). Furthermore, the direction of the anomalous zonal

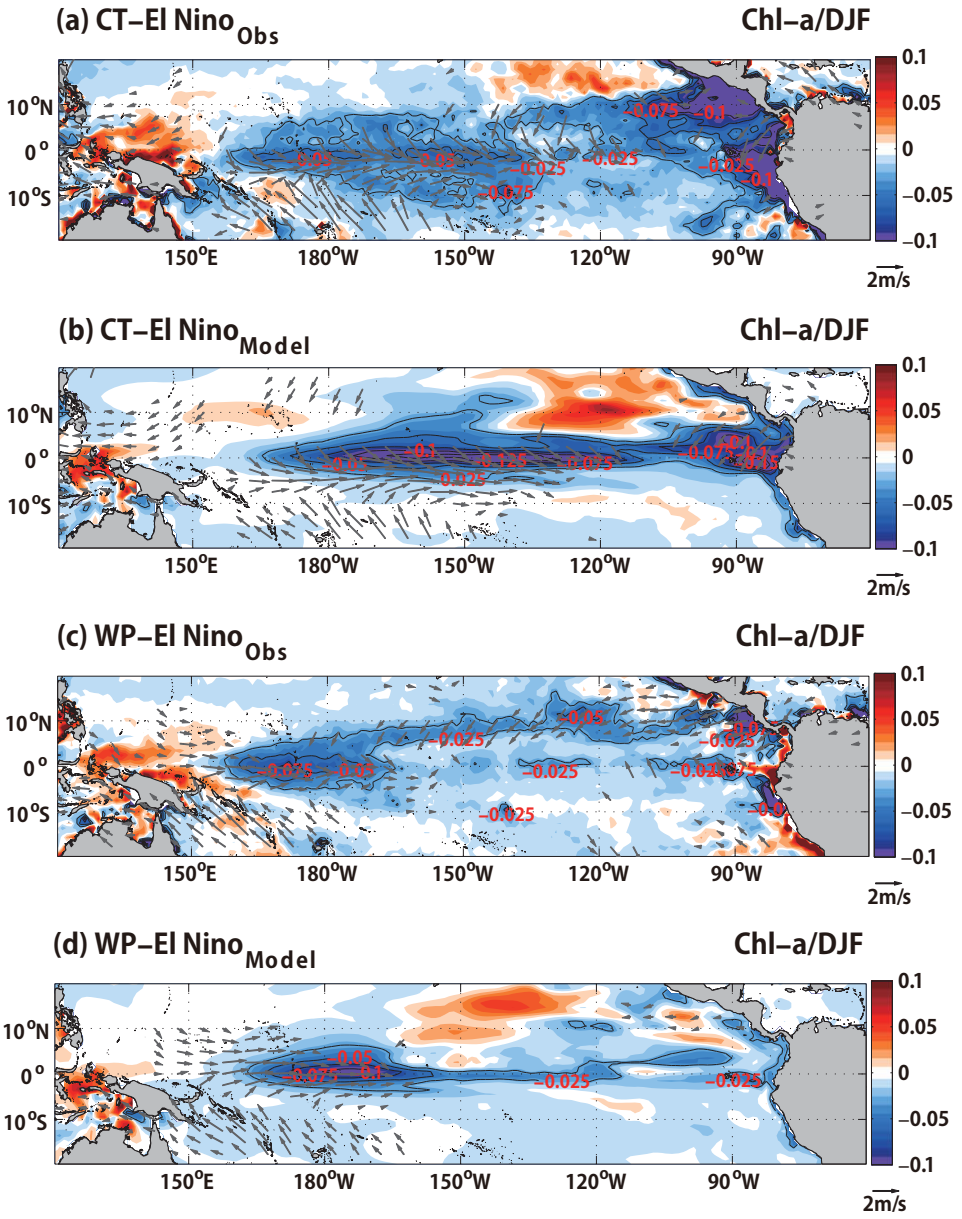

Figure 4. Observed chlorophyll anomaly composite (mg/m^3) during winter season (DJF) of El Niño events; (a) CT-El Niño for observation (1997–2010), (b) CT-El Niño for model (1971–2010), (c) WP-El Niño for observation, and (d) WP-El Niño for model. Dotted areas denote 95% confidence regions. Scale vector indicates 2 m/s. Only surface winds with velocity >0.5 m/s are shown.

current slowly changes, which is different from the CT-El Niño. Figures 5c and 5d are the same as in Figures 5a and 5b except the anomalous vertical velocity. In the CT-El Niño, anomalous vertical velocity is reduced during SON(0) in the eastern and central equatorial Pacific. And such a reduced upwelling still exists during the decaying period (i.e., February(1)-March(1)-April(1), FMA(1)) in the central equatorial Pacific. On the other hand, the reduction of upwelling is confined in the central equatorial Pacific in the WP-El Niño during SON(0) and the mature period (i.e., D(0)JF(1)). In particular, the maximum reduction of upwelling velocity is observed in the central equatorial Pacific during D(0)JF(1) in the WP-El Niño, which is contrast to the CT-El Niño.

We further analyze the evolution of the chlorophyll anomalies associated with two types of El Niño in our model (Figure 6). According to previous studies [*Kug et al*., 2009, 2010], the two types of El Niño events have a distinct evolution due to their different ocean adjustments. The CT-El Niño exhibits a relatively fast transition, due to the effective discharge process, compared to the WP-El Niño. Our model is able to capture

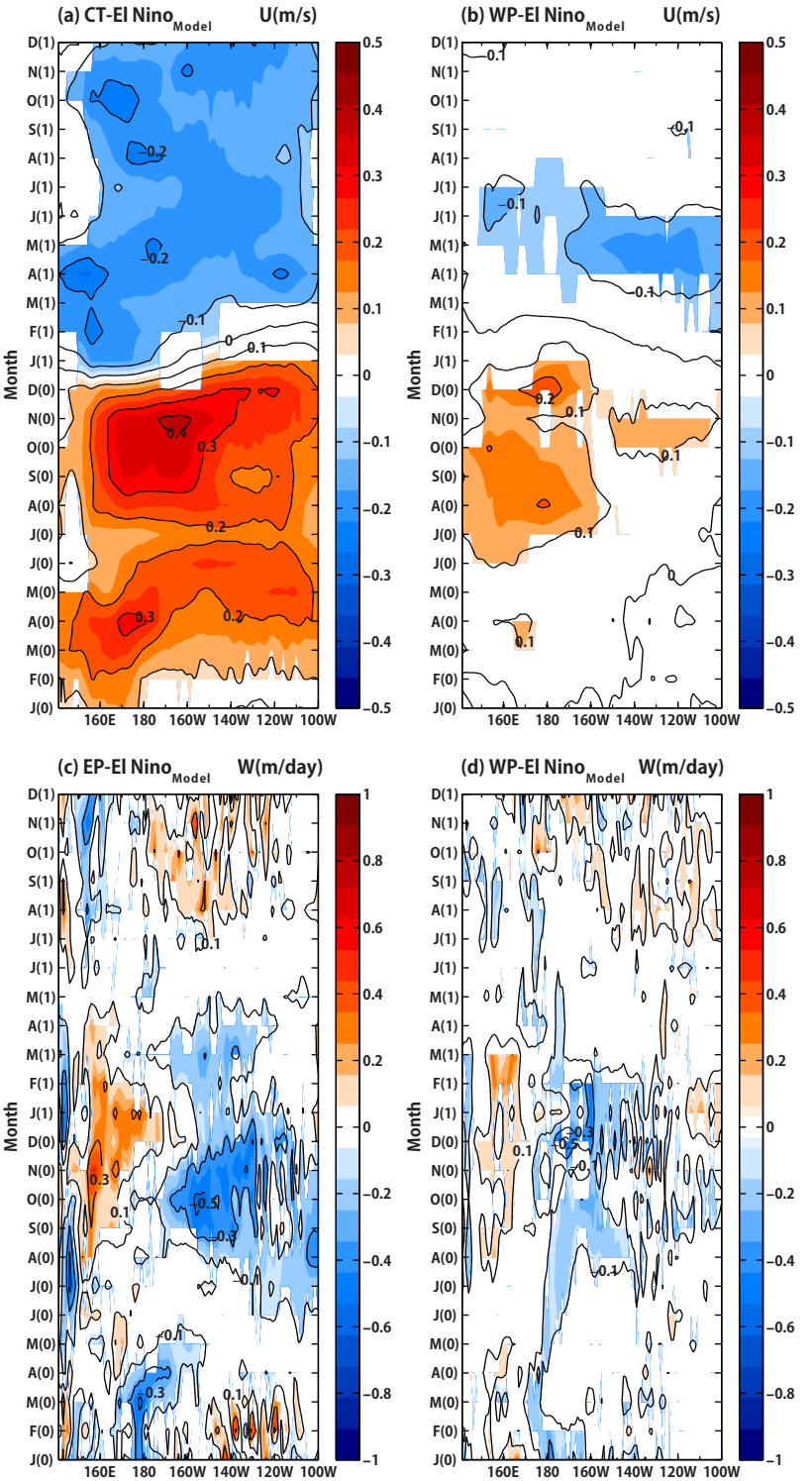

Figure 5. Longitude-time diagram of surface zonal current anomalies ((a) CT-El Niño and (b) WP-El Niño) and vertical velocity anomalies at the 50 m depth ((c) CT-El Niño and (d) WP-El Niño) in equatorial Pacific averaged over 2°S–2°N. Color bar scale is 0.1 m/s (U) and 0.1 m/d (W). Shaded areas denote 90% confidence regions.

the distinct evolution of the anomalous SST in the CT-El Niño (Figure 6a) and the WP-El Niño (Figure 6c). For the case of CT-El Niño, positive SST anomalies start to appear in the east, from 180°, during the previous spring (March(0)-April(0)-May(0), MAM(0)). They gradually develop with the progression of time, peaking

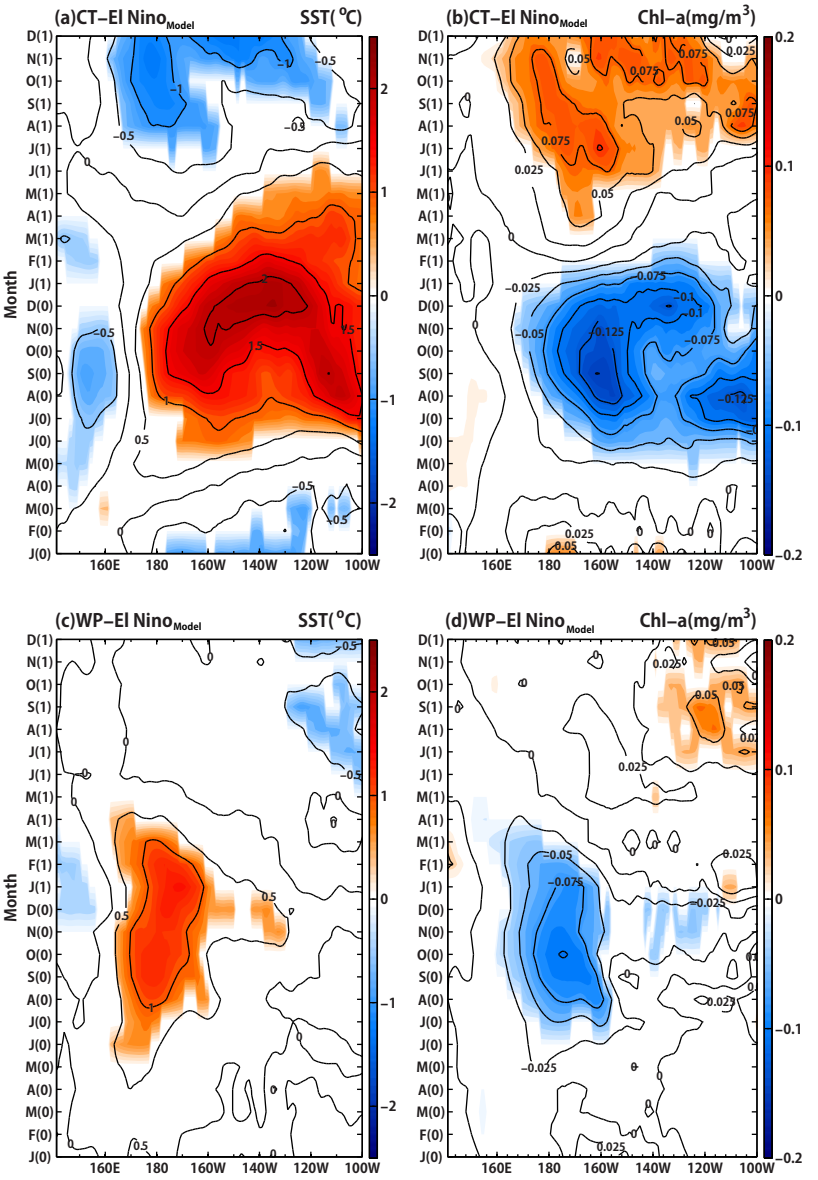

Figure 6. Longitude-time diagram of SST anomaly ((a) CT-El Niño and (c) WP-El Niño) and chlorophyll anomaly((b) CT-El Niño and (d) WP-El Niño) in equatorial Pacific averaged over 2°S–2°N. Contour interval is 0.5°C (SST) and 0.025 mg/m^3 (chlorophyll). Shaded areas denote 95% confidence regions.

during winter (D(0)JF(1)). After the peak season, positive SST anomalies rapidly decay and negative SST anomalies appear in the central equatorial Pacific during the following spring and summer (June(1)-July(1)-August(1), JJA(1)). In the WP-El Niño, meanwhile, positive SST anomalies developed during JJA(0), peaking during D(0)JF(1). In contrast to the CT-El Niño, the phase transition from positive to negative anomalies is relatively slow in the WP-El Niño.

These SST changes are closely linked to the changes in the chlorophyll concentration. As previously analyzed [*Blanchot et al.*, 1992; *Chavez*, 1999; *Radenac et al.*, 2005; *Ryan et al.*, 2006], it is evident that chlorophyll concentration decreases where SST warming takes place for both types of El Niño events. That is, there exist negative chlorophyll anomalies in the central and eastern equatorial Pacific in CT-El Niño events (Figure 6b) and they are confined within the central equatorial Pacific in WP-El Niño events (Figure 6d). However, the details of the temporal evolution of chlorophyll concentration are somewhat different from that of an anomalous SST. While the maximum positive SST anomalies appear during D(0)JF(1) in CT-El Niño, minimal negative chlorophyll anomalies appear during SON(0). This is because the mean chlorophyll concentration

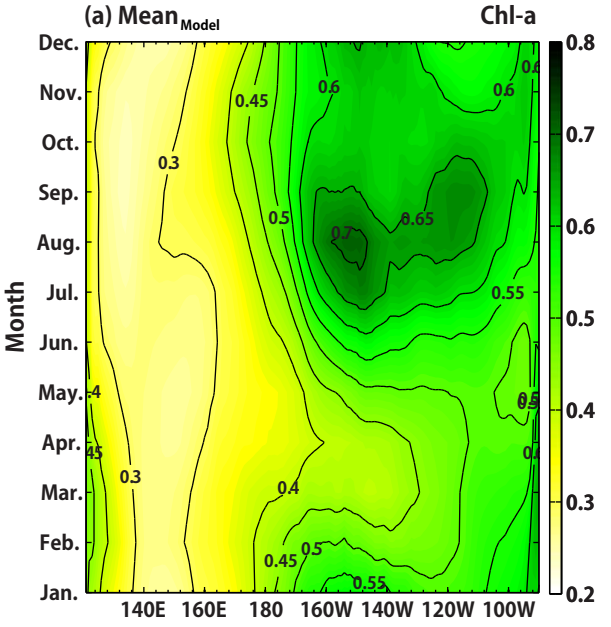

Figure 7. Longitude-time diagram of (a) mean chlorophyll (mg/m^3) in equatorial Pacific averaged over 2°S–2°N during 1971–2010.

is at its maximum during the fall (see Figure 7) when the anomalous upwelling is significantly reduced in the central equatorial Pacific (see Figure 5c). Therefore, the anomalous concentration of chlorophyll can also be large during SON(0), prior to the peak period for a CT-El Niño. In addition, the anomalous eastward current in the upper ocean can also be strong during SON(0) (see Figure 5a), indicating that the zonal advection of nutrient-poor water from the warm pool region plays a role in minimizing the chlorophyll concentration.

After a mature period of CT-El Niño, the negative anomalies of chlorophyll disappear very quickly, and the positive anomalies appear rapidly (Figure 6b). It is noteworthy that the negative anomalies of chlorophyll suddenly disappear in the central equatorial Pacific after a peak period of CT-El Niño, and positive anomalies start to appear during the following Feb(1), in spite of the presence of an anomalous warm SST during the same period (Figure 6a). This indicates that the transition of chlorophyll concentration associated with CT-El Niño events from the mature period to the decaying period tends to precede that of an anomalous SST by 2–3 months. Conversely, the evolution of chlorophyll anomalies is similar to that of an anomalous SST in the central equatorial Pacific (Figures 6c and 6d) in the WP-El Niño. In other words, a phase transition of the anomalous SST and chlorophyll from the mature period to the decaying period appears concurrently in the WP-El Niño. This indicates that the two types of El Niño have distinct biological responses, not only in terms of spatial patterns, but also temporal evolutions. As shown in Figure 5, a reduced upwelling and eastward zonal advection of warm pool water lead to the anomalous low chlorophyll during the developing period of the CT-El Niño. However, changes in the upwelling in the eastern equatorial Pacific are not effective in the WP-El Niño (see Figure 5d), because of the weak trade winds in the central equatorial Pacific (not shown). Therefore, we argue that zonal advection from less nutrient water affects the distribution of anomalous low chlorophyll in the WP-El Niño, as well as the CT-El Niño. Previous studies have also suggested that zonal advection is major process for chlorophyll response during WP-El Niño [*Radenac et al*., 2012; *Gierach et al*., 2012].

Figures 8a and 8b show the spatial structure of anomalous zonal current and chlorophyll concentration during SON(0) in the CT-El Niño and WP-El Niño events. The anomalous eastward current, which is averaged from surface to the depth of 50 m, is distinctive for both types of El Niño events, which is important in developing an anomalous SST. While the eastward current is only confined to the western-central equatorial Pacific in the WP El Niño, the current anomalies show a basin scale in the CT El Niño. It is quite striking that the pattern of the zonal current anomalies matched the anomalous chlorophyll concentration very well. This suggests that the anomalous zonal current plays a role to decrease chlorophyll concentration during the developing period of both types of El Niños, by advecting mean low chlorophyll concentration and nutrient-poor water from the western equatorial Pacific. Simulated model results have shown similar results based on observations [*Turk et al*., 2011; *Radenac et al*., 2012; *Gierach et al*., 2012]. Therefore, we argue that the anomalous low chlorophyll concentration is mainly due to both the advection of low chlorophyll concentration with less nutrient water (Figure 8) and the reduction during the transport due to nutrient limitation (see Figures 5 and 7). However, it is noteworthy that the anomalous high chlorophyll concentrations are observed to the west of 150°E during the CT-El Niño (1997/1998) and WP-El Niño (2002/2003) in the

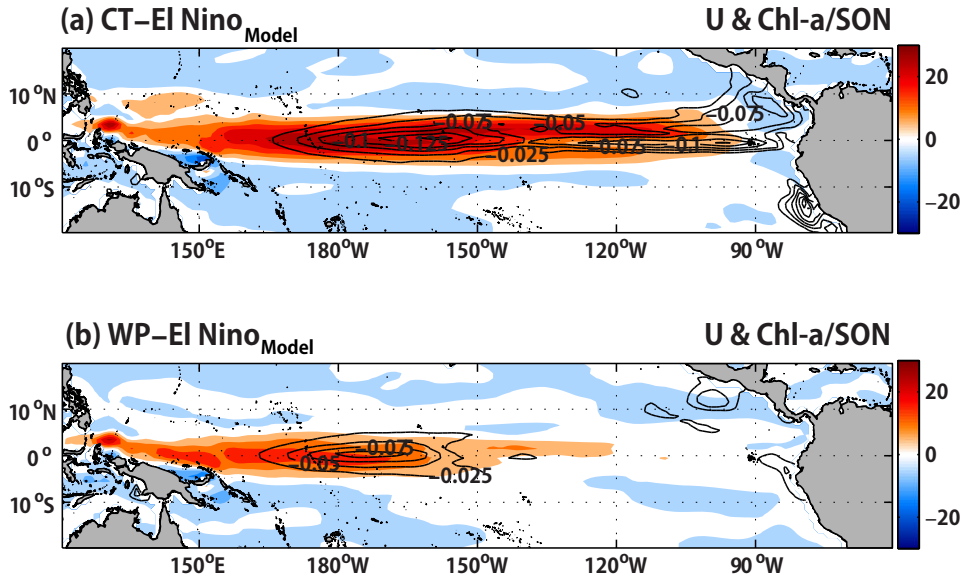

Figure 8. Composite of anomalous zonal current averaged vertically over surface ~50 m (shading) and chlorophyll anomaly (contour; only negative anomaly shown) during SON (0) ((a) CT-El Niño and (b) WP-El Niño). Shading interval is 5 cm/s and contour interval is 0.025 mg/m^3.

observation [see *Radenac et al*., 2012, Figures 6 and 7]. In addition, the anomalous chlorophyll concentration in the far western equatorial Pacific is not low in the model as shown in Figures 6b and 6d. Therefore, we speculate that the chlorophyll reduction during transport due to nutrient limitations is mainly associated with the anomalous low chlorophyll concentration during the developing period of both types of El Niños.

Our further analysis indicates that the distinct difference in the anomalous zonal currents between the two types of El Niño events can be explained by the geostrophic currents. During (D(0)JF(1)) in both types of El Niño events, the westerly wind stress forcings prevail over the central equatorial Pacific (not shown). Therefore, the sudden changes in the anomalous zonal current during the peak period in the CT-El Niño are not explained by changes in the Ekman currents. According to previous study [*An and Jin*, 2001], the equatorial mixed layer current can be divided into two components: (i) an Ekman current and (ii) a Geostrophic current. In the equatorial wave theory, the geostrophic balance is a good approximation for the momentum balance in the meridional direction [*Jin and An*, 1999]. That is, the meridional structure of the thermocline depth is directly linked to the equatorial geostrophic zonal current.

Figure 9 shows the meridional structure of the zonal mean (140°E–90°W) sea level anomalies associated with the two types of El Niño events in the model. Positive sea level anomalies indicate a deepening of the thermocline depth. According to *Jin an An* [1999], a positive sea level height anomaly precedes El Niño by about a quarter cycle of the ENSO period, and the water mass is discharged after the peak period of the El Niño. During SON(0) in the CT-El Niño (Figure 9a), strong positive sea level height prevails in the equatorial region, which is indicative of strong eastward geostrophic currents. After D(0)JF(1) in the CT-El Niño, the equatorial water mass rapidly discharges so that a strong negative sea level height anomaly appears. Such a rapid change in the sea level height explains the sudden change in the geostrophic currents' direction, which is consistent with the changes in the anomalous zonal current (shown in Figure 5a). However, the positive sea level anomalies begins to appear in July(0) in the WP-El Niño. Its growth is slow and its magnitude is weak. Changes in the anomalous sea level height begins to emerge the following March(1) after the peak period of the WP-El Niño, which is also consistent with the results shown in Figure 5b. Note that such evolutions of the zonal mean sea level associated with a two-type El Niño are consistent with the observational features [*Kug et al*., 2009].

3.2.2. Changes in Chlorophyll Concentration During the Decaying Period

As previously discussed, the chlorophyll responses to the two types of El Niño events are closely linked to the zonal current anomalies. In order to understand the details of the chlorophyll response after the peak period of the two types of El Niño events, we first examine the climatological distribution of chlorophyll,

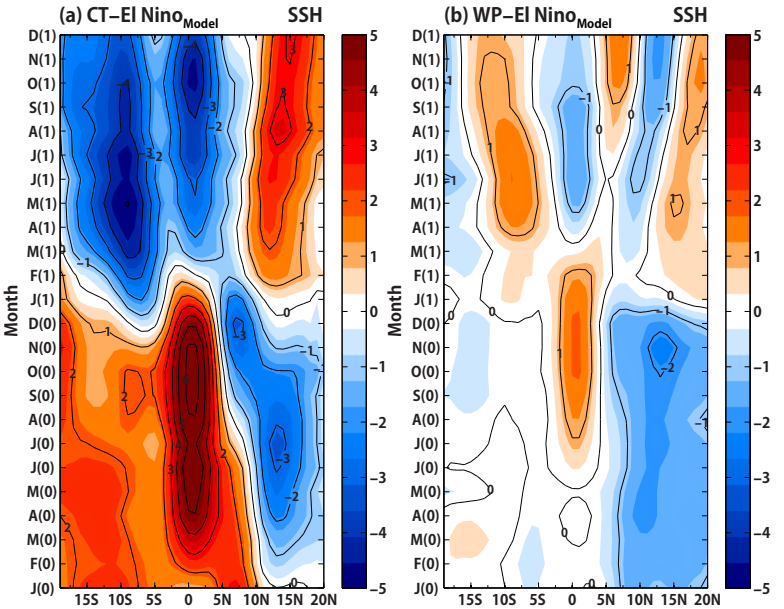

Figure 9. Latitude-time diagram of SSH anomaly in equatorial Pacific averaged over 140°E–90°W during (a) CT-El Niño and (b) WP-El Niño. Contour interval is 1 cm. Shaded areas denote 95% confidence regions.

nitrate, and dissolved iron along the equatorial region (150°E–80°W, averaged 2°N–2°S) for the years 1971–2010 (Figure 10). The restoration of chlorophyll is mainly affected by light, temperature, and nutrients. Except the Arctic region, the mean temperature is warm for the increase of chlorophyll; therefore, the chlorophyll concentration is limited by nutrients. The maximum chlorophyll concentration is observed between the MLD and the thermocline depth in the eastern equatorial Pacific (Figure 10a). Nitrate (NO_3) and iron (Fe) are two major nutrients to controlling phytoplankton growth in the tropical Pacific. NO_3 is enough in the eastern equatorial Pacific (east of 150°W) due to a shallow thermocline depth (Figure 10b). On the other hand, iron (Fe) concentration exists near in the far eastern and western equatorial Pacific (Figure 10c). In particular, a high concentration of iron is observed in the above thermocline depth in the far western equatorial Pacific, which is due to its transportation from the New Guinea shelf and eastern coastal upwelling [*Ryan et al*., 2006]

As shown in Figure 6, the sign of chlorophyll anomalies associated with the CT-El Niño abruptly changes from a negative to a positive in the central equatorial Pacific after its peak period. Conversely, the chlorophyll anomalies during the decaying period of the WP-El Niño are relatively low and show little to no changes in the central equatorial Pacific. These differences can be seen more clearly in vertical cross-section of the chlorophyll concentration (Figure 11). During the peak period ((D(0)JF(+1)) of the two types of El Niño events, both the WP-El Niño (Figure 11a) and the CT-El Niño (Figure 11b) have anomalous low chlorophyll concentrations around near date line or 150°W, respectively. Also, the anomalous low chlorophyll concentration appears around the MLD in both types of El Niño, indicating that the entrainment processes into the mixed layer play a key role to determine the chlorophyll concentration. Furthermore, negative anomalies weaken during MAM(+1) in the central equatorial Pacific, and then a weak positive anomaly starts to appear in the eastern equatorial Pacific in a WP-El Niño (Figure 11c). In contrast, the evolution of chlorophyll associated with a CT El Niño is dramatic. The strong negative anomalies over the entire Pacific basin suddenly disappear from D(0)JF(1) to MAM(+1). Positive anomalies of chlorophyll concentration seem to propagate to the east in the central equatorial Pacific (Figure 11d), which is associated with abrupt changes of chlorophyll concentration in the CT-El Niño.

To examine the origin of the positive chlorophyll anomalies in the western equatorial Pacific during MAM(1) in the CT-El Niño, the vertical distribution of nutrients and the zonal current associated with the CT-El Niño are displayed in Figure 12. During D(0)JF(1), the nutricline has not yet risen, due to the anomalous downwelling in the eastern equatorial Pacific, which caused an insufficient nutrients between the MLD and thermocline depth. Specifically, negative nitrate anomalies still exist in the central equatorial Pacific, which is

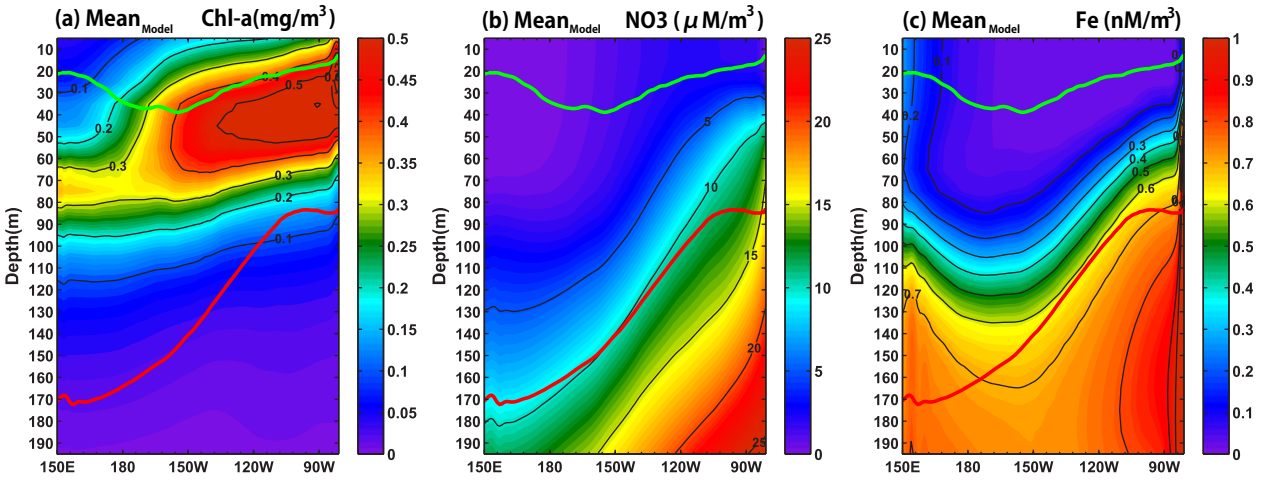

Figure 10. Vertical cross section of (a) Mean chlorophyll (mg/m^3); (b) Mean NO_3 (μM/L); and (c) mean dissolved iron (nM/L) averaged latitudinally over 2°S–2°N during 1971–2010. Contour interval is 0.1 mg/m^3 (chlorophyll), 5 μM/L (NO_3), and 0.1 nM/L (Fe_d). Green line denotes the mixed layer depth and red line is 20°C isothermal line (thermocline).

responsible for the strong negative chlorophyll anomalies (Figure 12a). During MAM(1), the negative nitrate anomalies are weakened, but are still evident (Figure 12b). The positive chlorophyll anomalies start to emerge at that time, suggesting that another factor plays a role in the development of positive chlorophyll during MAM(1). As shown in Figure 12c, there is an anomalous high concentration of dissolved iron in the

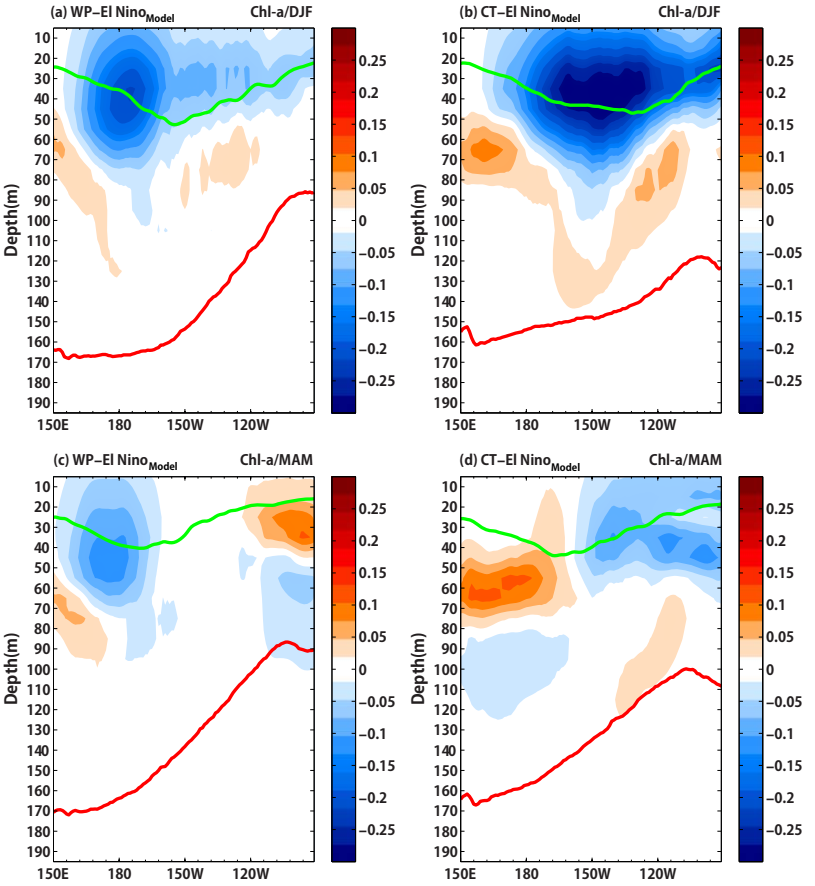

Figure 11. Vertical cross sections (averaged 2°S–2°N) of chlorophyll anomaly (mg/m^3) during decaying of El Niño; (a) DJF for WP-El Niño, (b) DJF for CT-El Niño, (c) MAM for WP-El Niño, and (d) MAM for CT-El Niño. Shades areas denotes 95% confidence region. Green (red) line indicates MLD (thermocline depth).

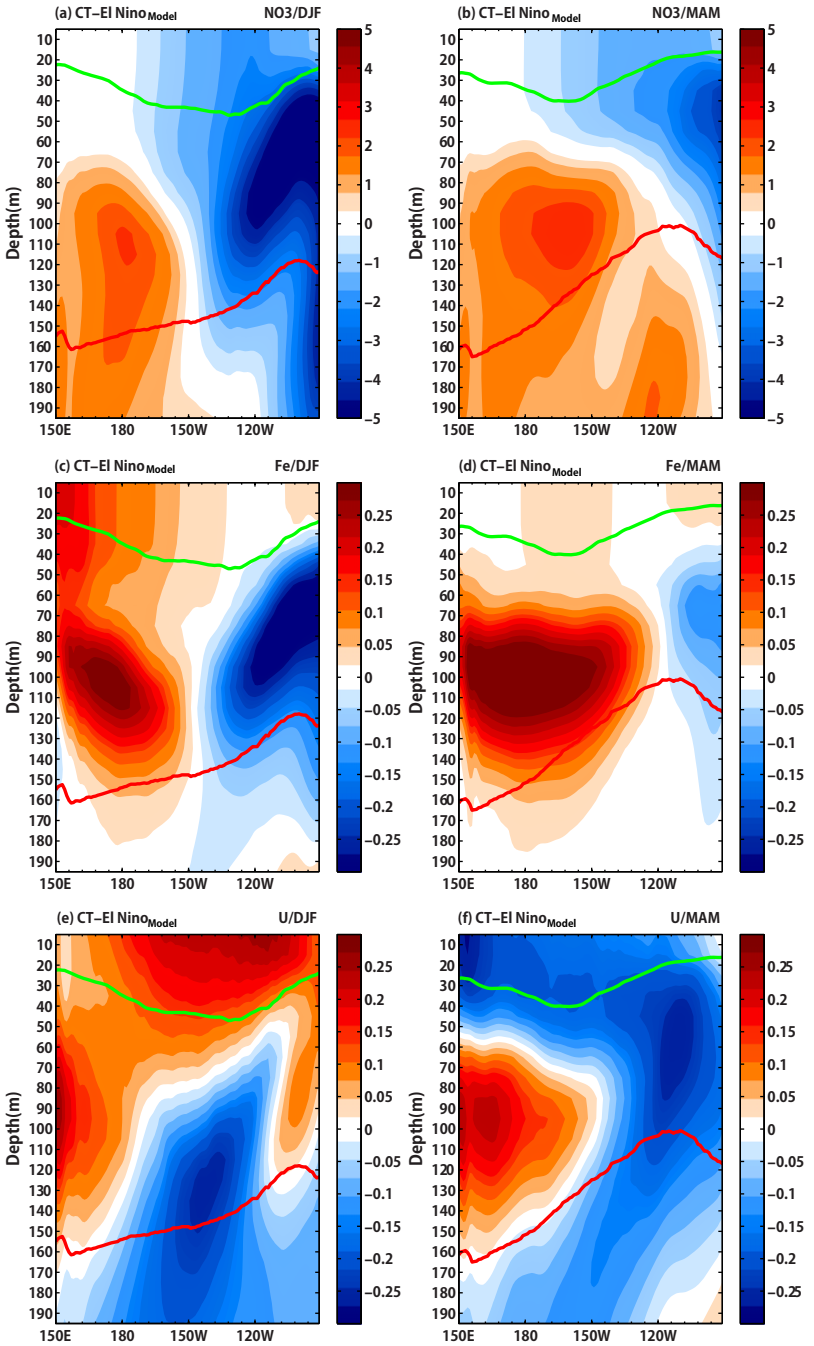

Figure 12. Vertical cross section (averaged 2°S–2°N) of nitrate anomaly (μM/L; (a) DJF and (b) MAM), dissolved iron anomaly (nM/L; (c) DJF and (d) MAM), U current anomaly (m/s; (e) DJF and (f) MAM) during CT-El Niño. Shades areas denotes 95% confidence region. Green (red) line indicates MLD (thermocline depth).

upper ocean in the western Pacific during D(0)JF(1). In the following MAM(1), the positive anomalies are further enhanced and expand to the central equatorial Pacific between the MLD and the thermocline depth, which can significantly contribute to chlorophyll concentration recovery. A similar pattern is also observed in the zonal current anomalies (Figures 12e and 12f). Because the concentration of the dissolved iron is higher near the western boundary (Figure 10c), the anomalous eastward currents lead to a positive advection of the dissolved iron.

Therefore, the anomalous eastward current in the subsurface layer of the western equatorial Pacific further develops and expands to the central equatorial Pacific during MAM(1) in the CT-El Niño (Figure 12f). In

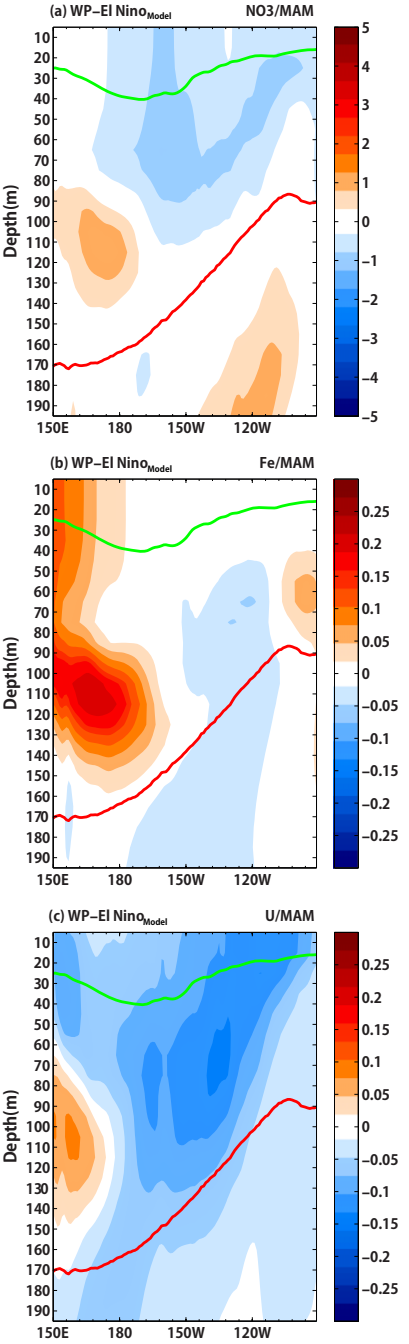

Figure 13. (a) Vertical cross section (averaged 2°S–2°N) of nitrate anomaly (μ*M*/L), (b) dissolved iron anomaly (n*M*/L), and (c) U current anomaly (m/s) during MAM(1) in the WP-El Niño. Green(red) line indicates MLD (thermocline depth).

addition, there exists a strong shear of zonal current below the MLD, which may lead a mixing to enhance the entrainment of iron and nitrate into the mixed layer. This acts to supply the dissolved iron to a photic layer over the central equatorial Pacific, which significantly contributes to the positive chlorophyll anomalies. Furthermore, we argue that the supply of dissolved iron from the far western equatorial Pacific is possible via the New Guinea Coastal Undercurrent (NGCU), as suggested by a previous study [*Wells et al*., 1999; *Radenac et al*., 2012]. In more detail, the NGCU plays a role to transports high-salinity waters from the Solomon Sea to the Equatorial Under Current (EUC) along the northern New Guinea margin [*Lindstrom et al*., 1987; *Tsuchiya et al*., 1989]. It is known that lithogenic input of iron to EUC source waters may occur through hydrothermal venting [*Gordon et al*., 1997], tectonic and volcanic processes [*Wells et al*., 1999], and fluvial flux, either directly from river outflow into the NGCU that flows close to the New Guinea coast or indirectly as river-borne sediments deposited on the shelf and upper slope are entrained by ocean margin circulation [*Milliman et al*., 1999; *Sholkovitz et al*., 1999; *Mackey et al*., 2002]. In addition, the role of tropical instability waves to contribute to the chlorophyll concentration has been also suggested by previous studies [*Friedrichs and Hofmann*, 2001; *Evans et al*., 2009; *Radenac et al*., 2012].

We also display the vertical distribution of nutrients and the zonal current associated with the WP-El Niño during MAM (1) (Figure 13). In contrast to the CT-El Niño, a shear of zonal current below the MLD is quite weak (Figure 13c). Subsequently, it leads a weak entrainment of iron and nitrate into the mixed layer by mixing processes. This acts to weaken the supply of the dissolved nitrate and iron (Figures 13a and 13b) to a photic layer over the central equatorial Pacific. In particular, the concentration of dissolved iron anomaly between the mixed layer depth and the thermocline depth is quite low during MAM(1) compared to the CT-El Niño (Figure 13b). These are associated with relatively slow transition of anomalous chlorophyll from the mature period to the decaying period in the WP-El Niño (see Figure 6d).

Finally, we examine details of the evolution of the sea level anomalies and undercurrent anomalies from the developing period to the decaying period in the CT-El Niño and WP-El Niño (Figure 14). The undercurrent is defined as the zonal current averaged over 70–150 m. During SON(0), a center of negative sea level anomalies appear off the equator in the eastern equatorial Pacific (Figure 14a); therefore, the anomalous EUC is weak in the western equatorial Pacific. During D(0)JF(1), the negative sea level anomalies in the Northern hemisphere are shifted to the equator, and developing further in the Southern hemisphere (Figure 14b). Such negative sea level anomalies induce the anomalous eastward undercurrent via a western boundary current in the equatorial western Pacific along

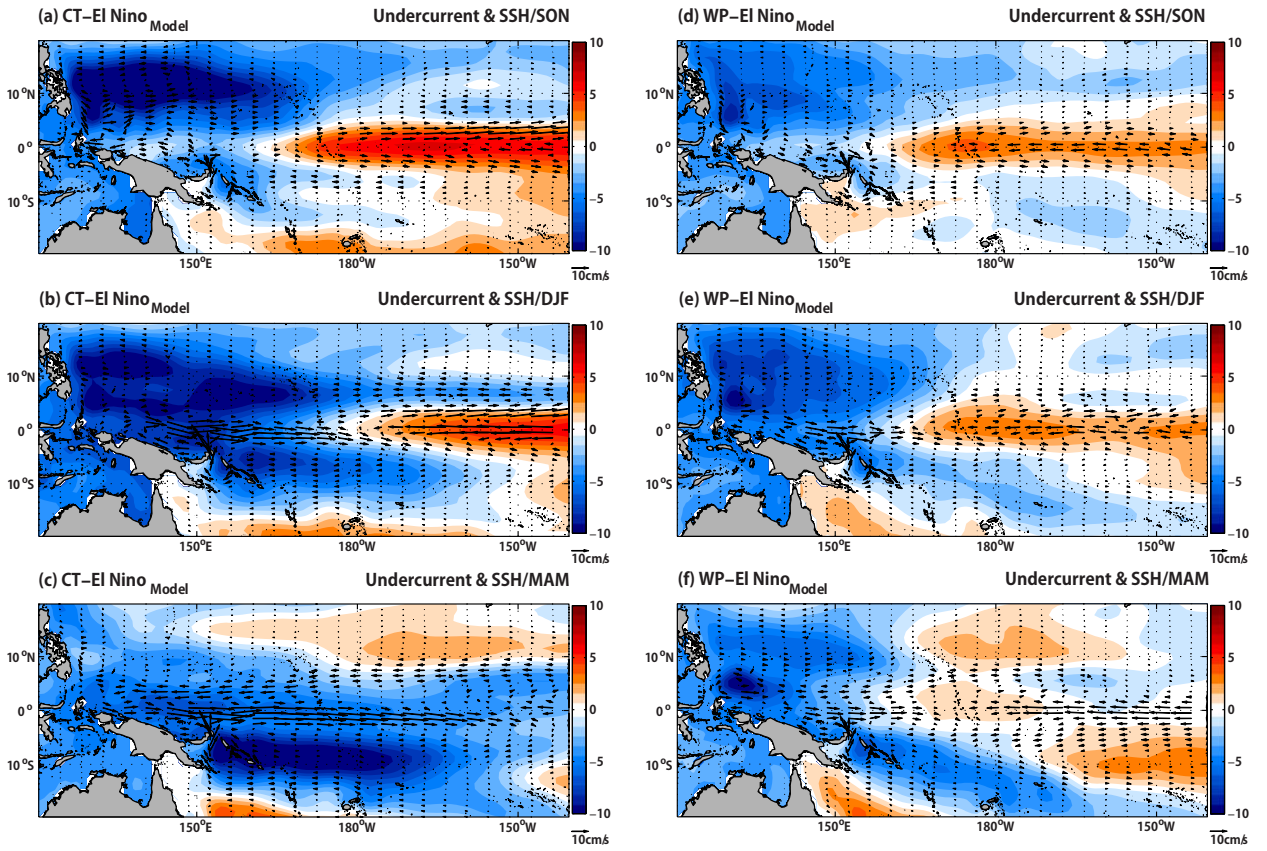

Figure 14. Composites of sea level (shading) and undercurrent (averaged 70–150 m; vector); for CT-El Niño (a) SON(0), (b) D(0)JF(+1), and (c) MAM(+1). (d–f) Same as Figures 14a–14c except the WP-El Niño. Contour interval is 1 cm and scale vector is 10 cm/s.

with the NGCU from Papua New Guinea, resulting in an enhanced eastward EUC. Concurrently, nutrients are transported by an enhanced the NGCU and EUC. In more details, it is well known in the literature that the EUC is a major source or iron in the equatorial Pacific and that it is suppressed during El Niño, but when the recovery period begins increases in chlorophyll concentrations are observed due to a return of the EUC [*Barber et al*., 1996; *Gordon et al*., 1997; *Chavez et al*., 1999; *Friedrichs and Hofmann*, 2001; *Radenac et al*., 2001, 2012; *Turk et al*., 2001].

Furthermore, the negative sea level anomalies mean a shallowing of nutricline in the western equatorial Pacific. Therefore, the positive chlorophyll anomalies begin to increase in the western equatorial Pacific during D(0)JF(1). During MAM(1), negative sea level anomalies spread east-southward, due to a westward wind-driven current and a geostrophic current (Figure 14c). This spread of negative sea level is able to enhance the EUC along with a rising of nutricline and a vertical position in the western and central equatorial Pacific. Therefore, we confirm that the restoration of chlorophyll in the CT-El Niño is mainly due to the zonal advection of iron associated with the EUC, which has been suggested by previous literature [*Radenac et al*., 2001; *Turk et al*., 2001; *Ryan et al*., 2006; *Radenac et al*., 2012]. On the other hand, the negative sea level anomalies in the Northern hemisphere is still dominant off the equator and its magnitude is weak in the Southern hemisphere during SON(0) and D(0)JF(1) in the WP-El Niño. This is associated with a weakening of eastward EUC through a western boundary current in the equatorial western Pacific along with the NGCU from Papua New Guinea, which is in contrast to the CT-El Niño. Furthermore, negative sea level anomalies are confined in the western tropical Pacific and a westward undercurrent is observed in the eastern tropical Pacific during MAM(1) in the WP-El Niño (Figure 14f). This prevents to enhance the EUC along with a rising of nutricline and a vertical position in the western and central equatorial Pacific, resulting in low concentration chlorophyll and its little changes in the central equatorial Pacific in the WP-El Niño. Note that, we also analyze the Simple Ocean Data Assimilation (SODA) data [*Carton and Giese*, 2008] and found that the SODA data set also show a similar evolution of the sea level anomalies and undercurrent anomalies comparable to the model (not shown).

4. Summary

The ENSO plays a key role in influencing the variability of chlorophyll in the tropical Pacific ecosystem. According to recent studies, a new type of El Niño (i.e., WP-El Niño) has occurred more frequently than the CT-El Niño during recent decades. Several previous studies which examined the Chlorophyll response to the two different types of El Niño using a satellite observation data [*Turk et al*., 2011; *Radenac et al*., 2012; *Gierach et al*., 2012] but the number of WP-El Niño events is limited because of data availability issues. We examined the chlorophyll response to the two types of El Niño events using a long-term ocean-biogeochemical coupled model simulation that utilizes GFDL MOM4p1, which is forced by the historical wind stress forcing from the years 1951 to 2010. Most previous studies pointed out the importance of horizontal advection in the central Pacific, which is confirmed in the present study based on a coupled model simulation. In addition, we also examined the details of mechanisms of the nutrients supply process associated with the amount of chlorophyll during the developing or decaying period in the two types of El Niño, which are distinguished from previous studies.

It is found that the ocean model is able to reasonably simulate the CT-El Niño and WP-El Niño events in terms of their amplitudes and spatial patterns compared to previous observations. However, the model shows a bias when simulating the center of the maximum positive westward anomalies for both types of El Niño events. In spite of discrepancies, the ocean model is able to reasonably simulate the distribution of chlorophyll concentrations and their interannual variability.

The relationship between SST and chlorophyll evolutions is different between CT-El Niño and WP-El Niño in terms of not only spatial patterns, but also temporal evolution. In the case of CT-El Niño, the maximum positive SST anomalies appear in the central and eastern equatorial Pacific during the peak period of the CT-El Niño during winter, which is in contrast with the peak of negative chlorophyll anomalies during the previous fall. This is mainly associated with the anomalous eastward zonal advection, which brings less nutrient water from the warm pool region during the previous fall. Therefore, the transition of chlorophyll concentration, which is associated with the decaying period of the CT-El Niño, tends to precede that of the anomalous SST by 2–3 months. In the case of WP-El Niño, negative chlorophyll anomalies are confined within the central equatorial Pacific during the developing period. It is found that the evolution of chlorophyll anomalies is similar to that of the anomalous SST in the central equatorial Pacific from the developing period to the decaying period in the WP-El Niño.

To investigate the details of the role of zonal current in the evolution of chlorophyll after the peak period of two types of El Niño events, the evolution of mixed layer zonal current anomalies are examined. We found that the distinct difference in the evolution of anomalous zonal current between the two types of El Niño events can be explained by the geostrophic current, which has not been explained in previous studies. Further investigation indicated that the anomalous zonal current responsible for dramatic changes in the chlorophyll concentration during the decaying period of CT-El Niño acts to advect high chlorophyll and rich nutrients from the eastern Pacific and supplies the dissolved iron to a photic layer over the central equatorial Pacific via the NGCU, which is in contrast to the WP-El Niño. Chlorophyll blooming is significantly correlated with a shoaling of the thermocline and the EUC in the western and central tropical Pacific during El Nino/La Nina transitions [*Gierach et al*., 2013].

We investigated the chlorophyll responses to the two types of El Niño events using the simulation of an ocean model forced by historical winds. To fully understand the chlorophyll responses to the two types of El Niño events, however, a full atmosphere-ocean coupled model is necessary. This is because there exist biological feedback processes between the ENSO and the ecosystem in the tropical Pacific [*Timmermann and Jin*, 2002; *Park et al*., 2011]. Further research on the feedback processes between chlorophyll variability and the two types of El Niño ENSO using a fully coupled model is needed.

Acknowledgment
This work was supported by the National Research Foundation of Korea grant funded by the Korean Government (MEST) (NRF-2009-C1AAA001–2009-0093042).

References

AchutaRao, K., and K. Sperber (2002), Simulation of the El Niño southern oscillation: Results from the coupled model intercomparison project, *Clim. Dyn.*, *19*, 191–209.

An, S. I., and F.-F. Jin (2001), Collective role of thermocline and zonal advective feedbacks in the ENSO mode, *J. Clim.*, *14*, 3421–3432, doi: 10.1175/1520-0442(2001)014<3421:CROTAZ>2.0.CO;2.

Ashok, K., S. K. Behera, S. A. Rao, H. Weng, and T. Yamagata (2007), El Niño Modoki and its possible teleconnections, *J. Geophys. Res.*, *112*, C11007, doi:10.1029/2006JC003798.

Barber, R. T., M. P. Sanderson, S. T. Lindley, F. Chai, J. Newton, C. C. Trees, D. G. Foley, and F. P. Chavez (1996), Primary productivity and its regulation in the equatorial Pacific during and following the 1991–1992 El Niño, *Deep Sea Res., Part II*, *43*, 933–969.

Behrenfeld, M. J., et al. (2001), Biospheric primary production during an ENSO transition, *Science*, *291*, 2594–2597, doi:10.1126/science.1055071.

Blanchot, J., M. Rodier, and A. Le Bouteiller (1992), Effect of El Niño Southern Oscillation events on the distribution and abundance of phytoplankton in the Western Pacific Tropical Ocean along 165°E, *J. Plankton Res.*, *4*, 137–156.

Campbell, J. W., J. M. Blaisdell, and M. Darzi (1995), Level-3 SeaWiFS data products: Spatial and temporal binning algorithms, *NASA Tech. Memo. 104566*, NASA Goddard Space Flight Center, Greenbelt, Md. vol. *32*, 80 pp.

Carton, J. A., and B. S. Giese (2008), A reanalysis of ocean climate using simple ocean data assimilation (SODA), *Mon. Weather Rev.*, *136*, 2999–3017.

Chavez, F. F., P. G. Strutton, G. E. Friederich, R. A. Feely, G. C. Feldman, D. G. Foley, and M. J. McPhaden (1999), Biological and chemical response of the equatorial Pacific Ocean to the 1997–1998 El Niño, *Science*, *286*, 2126–2131, doi:10.1126/science.286.5447.2126.

Chavez, F. P., K. R. Buck, K. H. Coale, J. H. Martin, G. R. DiTullio, N. A. Welschmeyer, A. C. Jacobson, and R. T. Barber (1991), Growth rates, grazing, sinking, and iron limitation of equatorial Pacific phytoplankton, *Limnol. Oceanogr.*, *36*, 1816–1833.

Chavez, F. P., P. G. Strutton, and M. J. McPhaden (1998), Biological-physical coupling in the central Pacific during the onset of the 1997–98 El Niño, *Geophys. Res. Lett.*, *25*, 3543–3546.

Chavez, F. P., J. Ryan, S. E. Lluch-Cota, and M. Niquen (2003), From anchovies to sardines and back: Multidecadal change in the Pacific Ocean, *Science*, *299*, 217–221, doi:10.1126/science.1075880.

Cullen, J. J. (1991), Hypotheses to explain high-nutrient conditions in the open sea, *Limnol. Oceanogr.*, *36*, 1578–1599.

Dandonneau, Y., P. Y. Deschamps, J. M. Nicolas, H. Loisel, J. Blanchot, Y. Montel, F. Thieuleux, and G. Bécu (2004), Seasonal and interannual variability of ocean color and composition of phytoplankton communities in the North Atlantic, equatorial Pacific and South Pacific, *Deep Sea Res., Part II*, *51*, 303–318.

Doty, M. S., and M. Oguri (1956), The island mass effect, *J. Int. Counc. Explor. Sea*, *22*, 33–37.

Dunne, J. P. (1999), Measured and modeled particle export in equatorial and coastal upwelling regions, PhD thesis, 167 pp., Univ. of Washington, Seattle.

Dunne, J. P., J. W. Murray, M. Rodier, and D. A. Hansell (2000), Export flux in the western and central equatorial Pacific: Zonal and temporal variability, *Deep Sea Res., Part I*, *47*, 901–936.

Dunne, J. P., R. A. Armstrong, A. Gnanadesikan, and J. L. Sarmiento (2005), Empirical and mechanistic models for the particle export ratio, *Global Biogeochem. Cycles*, *19*, B4025, doi:10.1029/2004GB002390.

Dunne, J. P., A. Gnanadesikan, J. L. Sarmiento, and R. D. Slater (2010), Technical description of the prototype version (v0) of Tracers Of Phytoplankton with Allometric Zooplankton (TOPAZ) ocean biogeochemical model as used in the Princeton IFMIP model, *Biogeoscience*, *7*, 3593–3624.

Evans, W. W., P. G. Strutton, and F. P. Chavez (2009), Impact of tropical instability waves on nutrient and chlorophyll distributions in the equatorial Pacific, *Deep Sea Res., Part I*, *56*, 178–188.

Field, C. B., M. J. Behrenfeld, J. T. Randerson, and P. Falkowski (1998), Primary production of the biosphere: Integrating terrestrial and oceanic components, *Science*, *281*, 237–240, doi:10.1126/science.281.5374.237.

Friedrichs, M. A. M., and E. E. Hofmann (2001), Physical control of biological processes in the central equatorial Pacific Ocean, *Deep Sea Res., Part I*, *48*, 1023–1069.

Geider, R. J., H. L. MacIntyre, and T. M. Kana (1996) A dynamic model of photoadaptation in phytoplankton, *Limnol. Oceanogr.*, *41*(1), 1–15.

Gierach, M. M., T. Lee, D. Turk, and M. J. McPhaden (2012), Biological response to the 1997–98 and 2009–10 El Niño events in the equatorial Pacific Ocean, *Geophys. Res. Lett.*, *39*, L10602, doi:10.1029/2012GL051103.

Gierach, M. M., M. Messié, T. Lee, K. B. Karnauskas, and M.-H. Radenac (2013), Biophysical Responses near Equatorial Islands in the Western Equatorial Pacific Ocean during El Niño/La Niña Transitions, *Geophys. Res. Lett.*, *40*, 5473–5479, doi:10.1002/2013GL057828.

Ginoux, P., M. Chin, I. Tegen, J. M. Prospero, B. Holben, O. Dubovik, and S.-J. Lin (2001), Sources and distributions of dust aerosols simulated with the GOCART model, *J. Geophys. Res.*, *106*, 20,255–20,274.

Gnanadesikan, A., et al. (2006), GFDL's CM2 global coupled climate models: Part II: The baseline ocean simulation, *J. Clim.*, *19*, 675–697.

Gnanadesikan, A., J. P. Dunne, and J. John (2011), What ocean biogeochemical models can tell us about bottom-up control of ecosystem variability, *ICES J. Mar. Sci.*, *68*, 1030–1044, doi:10.1093/icesjms/fsr068.

Gordon, R. M., K. H. Coale, and K. S. Johnson (1997), Iron distribution in the equatorial Pacific: Implications for new production, *Limnol. Oceanogr.*, *43*, 419–431.

Griffies, S. M., M. Schmidt, and M. Herzfeld (2009), Elements of mom4p1, *GFDL Ocean Group Tech. Rep. 6*, Princeton, N. J. pp. 444.

Hannachi, A., D. Stephenson, and K. Sperber (2003), Probability-based methods for quantifying nonlinearity in the ENSO, *Clim. Dyn.*, *20*, 241–256, doi:10.1007/s00382-002-0263-7.

Henson, S. A., J. L. Sarmiento, J. P. Dunne, L. Bopp, I. Lima, S. C. Doney, J. John, and C. Beaulieu (2009), Is global warming already changing ocean productivity?, *Biogeosci. Discuss.*, *6*, 10,311–10,354.

Jin, D., D. E. Waliser, C. Jones, and R. Murtugudde (2013), Modulation of tropical ocean surface chlorophyll by the Madden-Julian Oscillation, *Clim. Dyn.*, *40*, 39–58, doi:10.1007/s00382-012-1321-4.

Jin, F.-F., and S.-I. An (1999), Thermocline and zonal advective feedbacks within the equatorial ocean recharge oscillator model for ENSO, *Geophys. Res. Lett.*, *26*, 2989–2992.

Kalnay, E., et al. (1996), The NCEP/NCAR 40-year reanalysis project, *Bull. Am. Meteorol. Soc.*, *77*, 437–471.

Kao, H.-Y., and J.-Y. Yu (2009), Contrasting eastern-Pacific and central-Pacific types of ENSO, *J. Clim.*, *22*, 615–632.

Kim, W., S.-W. Yeh, J.-H. Kim, J.-S. Kug, and M. Kwon (2011), The unique 2009–2010 El Niño event: A fast phase transition of warm pool El Niño to La Niña, *Geophys. Res. Lett.*, *38*, L15809, doi:10.1029/2011GL048521.

Kug, J.-S., F.-F. Jin, and S.-I. An (2009), Two types of El Niño events: Cold tongue El Niño and warm pool El Niño, *J. Clim.*, *22*, 1499–1515, doi:10.1175/2008JCLI2624.1.

Kug, J.-S., J. Choi., S.-I. An, F.-F. Jin, and A. T. Wittenberg (2010), Warm pool and Cold Tongue El Niño Events as Simulated by the GFDL 2.1 Coupled GCM, *J. Clim.*, *23*, 1226–1239, doi:10.1175/2009JCLI3293.1.

Landry, M. R., et al. (1997), Iron and grazing constraints on primary production in the central equatorial Pacific: An EqPac synthesis, *Limnol. Oceanogr.*, *42*, 405–418.

Large, W., and S. Yeager, (2004), Diurnal to decadal global forcing for ocean and sea-ice models: The data sets and flux climatologies, *NCAR Tech. Note NCAR/TN-460+STR*, CGD Div. of the Natl. Cent. for Atmos. Res., Boulder, Colo.

Lee, T., and M. J. McPhaden (2010), Increasing intensity of El Niño in the central-equatorial Pacific, *Geophys. Res. Lett.*, *37*, L14603, doi: 10.1029/2010GL044007.
Lewis, M. R., M. E. Carr, G. C. Feldman, W. Esaias, and C. McClain (1990), Influence of penetrating solar-radiation on the heat-budget of the equatorial Pacific-ocean, *Nature*, *347*, 543–545, doi:10.1038/347543a0.
Lewis, S. F., W. F. Taylor, R. M. Graham, W. A. Pettinger, J. E. Chutte, and C. G. Blomqvist (1983), Cardiovascular responses to exercise as functions of absolute and relative workload, *J. Appl. Physiol.*, *54*, 1314–1323.
Lindstrom, E. R., R. Lucas, R. Fine, E. Firing, S. Godfrey, G. Meyers, and M. Tsuchiya (1987), The western equatorial pacific ocean study, *Nature*, *330*, 533–537.
Livezey, R. E., and W. Y. Chen (1983), Statistical field significance and its determination by Monte-Carlo techniques, *Mon. Weather Rev.*, *111*, 46–59.
Mackey, D. J., J. E. O'Sullivan, and R. J. Watson (2002), Iron in the western Pacific: A riverine or hydrothermal source for iron in the Equatorial Undercurrent?, *Deep Sea Res., Part I*, *49*, 877–893.
Manizza, M., C. Le Quéré, A. J. Watson, and E. T. Buitenhuis (2005), Biooptical feedbacks among phytoplankton, upper ocean physics and sea-ice in a global model, *Geophys. Res. Lett.*, *32*, L05603, doi:10.1029/2004GL020778.
Mantua, N. J., S. R. Hare, Y. Zhang, J. M. Wallace, and R. C. Francis (1997), A Pacific interdecadal climate oscillation with impacts on salmon production, *Bull. Am. Meteorol. Soc.*, *78*, 1069–1079, doi:10.1175/1520-0477(1997)078<1069:APICOW>2.0.CO;2.
Martinez, E., and K. Maamaatuaiahutapu (2004), Island mass effect in the Marquesas Islands: Time variation, *Geophys. Res. Lett.*, *31*, L18307, doi:10.1029/2004GL020682.
McClain, C. R., G. C. Feldman, and S. B. Hooker (2004), An overview of the SeaWiFS project and strategies for producing a climate research quality global ocean bio-optical time series, *Deep Sea Res., Part II*, *51*, 5–42, doi:10.1016/j.dsr2.2003.11.001.
Milliman, J. D., K. L. Farnsworh, and C. S. Albertin (1999), Flux and fate of fluvial sediments leaving large islands in the East Indies, *J. Sea Res.*, *41*, 97–107.
Park, J.-Y., and J.-S. Kug (2013), Marine biological feedback associated with Indian Ocean Dipole in a coupled ocean/biogeochemical model, *Clim. Dym.*, *42*, 329–343, doi:10.1007/s00382-012-1640-5.
Park, J.-Y., J.-S. Kug, J.-S. Park, S.-W. Yeh, and C. J. Jang (2011), Variability of chlorophyll associated with ENSO and its possible biological feedback in the Equatorial Pacific, *J. Geophys. Res.*, *116*, C10001, doi:10.1029/2011JC007056.
Radenac, M.-H., C. Menkes, J. Vialard, C. Moulin, Y. Dandonneau, T. Delcroix, C. Dupouy, A. Stoens, and P.-Y. Deschamps (2001), Modeled and observed impacts of the 1997–1998 El Niño on nitrate and new production in the equatorial Pacific, *J. Geophys. Res.*, *106*, 26,879–26,898.
Radenac, M.-H., Y. Dandonneau, and B. Blanke (2005), Displacements and transformations of nitrate-rich and nitrate-poor water masses in the tropical Pacific during the 1997 El Niño, *Ocean Dyn.*, *55*, 34–46, doi:10.1007/s10236-005-0111-5.
Radenac, M.-H., F. Léger, A. Singh, and T. Delcroix (2012), Sea surface chlorophyll signature in the tropical Pacific during eastern and central Pacific ENSO events, *J. Geophys. Res.*, *117*, C04007, doi:10.1029/2011JC007841.
Radenac, M.-H., M. Messie, F. Leger, and C. Bosc (2013), A very oligotrophic zone observed from space in the equatorial Pacific warm pool, *Remote Sens. Environ.*, *134*, 224–233, doi:10.1016/j.rse.2013.03.007.
Ryan, J. P., I. Ueki, Y. Chao, H. Zhang, P. S. Polito, and F. P. Chavez (2006), Western Pacific modulation of large phytoplankton blooms in the central and eastern equatorial Pacific, *J. Geophys. Res.*, *111*, G02013, doi:10.1029/2005JG000084.
Sholkovitz, E. R., H. Elderfield, R. Szymczak, and K. Casey (1999), Island weathering: River sources of rare earth elements to the western Pacific Ocean, *Mar. Chem.*, *68*, 39–57.
Siegel, D. A., A. F. Michaels, M. C. O'Brien, and M. A. Hammer (1995), Seasonal variability of light availability and its utilization in the Sargasso Sea, *J. Geophys. Res.*, *100*, 8695–8713.
Smith, T. M., R. W. Reynolds, T. C. Peterson, and J. Lawrimore (2008), Improvements to NOAA's historical merged land-ocean surface temperature analysis (1880–2006), *J. Clim.*, *21*(10), 2283–2296.
Tilman, D. (1982), *Resource Competition and Community Structure*, Princeton Univ. Press, Princeton, N. J.
Timmermann, A., and F.-F. Jin (2002), Phytoplankton influences on tropical climate, *Geophys. Res. Lett.*, *29*(23), 2104, doi:10.1029/2002GL015434.
Trenberth, K. E., and D. P. Stepaniak (2001), Indices of El Niño evolution, *J. Clim.*, *14*, 1697–1701.
Tsuchiya, M., R. Lukas, R. A. Fine, E. Firing, and E. Lindstrom (1989), Source waters of the Pacific Equatorial Undercurrent, *Prog. Oceanogr.*, *23*, 101–147.
Turk, D., M. R. Lewis, G. W. Harrison, T. Kawano, and I. Asanuma (2001), Geographical distribution of new production in the western/central equatorial Pacific during El Niño and non-El Niño conditions, *J. Geophys. Res.*, *106*, 4501–4515.
Turk, D., C. S. Meinen, D. Antoine, M. J. McPhaden, and M. R. Lewis (2011), Implications of changing El Niño patterns for biological dynamics in the equatorial Pacific Ocean, *Geophys. Res. Lett.*, *38*, L23603, doi:10.1029/2011GL049674.
Wells, M. L., G. K. Vallis, and E. A. Silver (1999), Tectonic processes in Papua New Guinea and past productivity in the eastern equatorial Pacific Ocean, *Nature*, *398*(6728), 601–604.
Wittenberg, A. T., A. Rosati, N.-C. Lau, and J. J. Ploshay (2006), GFDL's CM2 global coupled climate models. PartIII: Tropical Pacific climate and ENSO, *J. Clim.*, *19*, 698–722.
Yeh, S.-W., J.-S. Kug, B. Dewitte, M.-H. Kwon, B. Kirtman, and F.-F. Jin (2009), El Niño in a changing climate, *Nature*, *461*, 511–514, doi: 10.1038/nature08316.
Yeh, S.-W., B. P. Kirtman, J.-S. Kug, W. Park, and M. Latif (2011), Natural variability of the central Pacific El Niño event on multi-centennial time scales, *Geophys. Res. Lett.*, *38*, L02704, doi:10.1029/2010GL045886.
Yoder, J. A., and M. Kennelly (2003), Seasonal and ENSO variability in global ocean phytoplankton chlorophyll derived from 4 years of SeaWiFS measurements, *Global Biogeochem. Cycles*, *17*(4), 1112, doi:10.1029/2002GB001942.
Yu, J.-Y., M.-M. Lu, and S.-T. Kim (2012), A change in the relationship between tropical central Pacific SST variability and the extratropical atmosphere around 1990, *Environ. Res. Lett.*, *7*, 034025.